ORIGINAL ARTICLE

ORAL DISEASES | WILEY

Heterogeneity of fibroblasts from radicular cyst influenced osteoclastogenesis and bone destruction

Jingwen Yang[1,2,3,4] | Shuyu Xu[5] | Hai-Cheng Wang[6] (iD)

[1]Department of Prosthodontics, Peking University School and Hospital of Stomatology, Beijing, China

[2]National Engineering Laboratory for Digital and Material Technology of Stomatology, Beijing, China

[3]Research Center of Engineering and Technology for Digital Dentistry of Ministry of Health, Beijing, China

[4]Beijing Key Laboratory of Digital Stomatology, Beijing, China

[5]Department of Oral Implant, School & Hospital Stomatology, Shanghai Engineering Research Center of Tooth Restoration and Regeneration, Tongji University, Shanghai, China

[6]Department of Pathology, School & Hospital of Stomatology, Shanghai Engineering Research Center of Tooth Restoration and Regeneration, Tongji University, Shanghai, China

Correspondence
Hai-Cheng Wang, Department of Pathology, School & Hospital of Stomatology, Tongji University, Shanghai Engineering Research Center of Tooth Restoration and Regeneration, 399 Middle Yanchang Road, Shanghai 200072, China.
Email: haichengwang@sina.com

Abstract

Aim: To analyze the heterogeneity of fibroblasts isolated from the fibrous capsules of radicular cysts and explore the effects of fibroblast subsets on bone destruction.

Methodology: Radicular cysts were divided into groups according to varying perilesional sclerosis identified by radiograph. Colony-forming units (CFUs) were isolated from the fibrous capsules of cysts, by which Trap + MNCs were induced, and the expression of osteoclastogenesis-related genes was compared among groups by real-time PCR. The variances in gene profiles of CFUs were identified by principal component analysis, and then, CFUs were divided into subsets using cluster analysis. The induction of Trap + MNCs and related gene expression was compared among subsets, and osteoclastogenic induction was blocked by IST-9 or bevacizumab. The fibroblast subsets in cysts were investigated by retrospective immunostaining with IST-9, VEGF-A, and CD34. A fibroblast subset that underwent gene editing by CRISPR/Cas was injected into the site of bone defects in animal models, and the in vivo effects on osteoclastogenesis were investigated.

Results: The fibroblast CFUs isolated from radicular cysts with perilesional unsclerotized cysts induced more Trap + MNCs than those with perilesional sclerotic cysts ($p < .05$). Most fibroblast CFUs from unsclerotized cysts belonged to Cluster 2, which induced more Trap + MNCs ($p < .05$) and highly expressed genes facilitating osteoclastogenesis; these results were different from those of Cluster 1 ($p < .05$), in which most CFUs were isolated from perilesional sclerotic cysts or controls ($p < .05$). The high expression of EDA + FN and VEGF-A was investigated in both the fibroblasts of Cluster 2 and the fibrous capsules of unsclerotized cysts ($p < .05$), and the number of Trap + MNCs induced by Cluster 2 was decreased by treatment with IST-9 and bevacizumab ($p < .05$). Consistently, EDA exon exclusion significantly decreased the osteoclastogenic induction of fibroblasts from Cluster 2 in vivo ($p < .05$).

Conclusion: The fibrous capsules of radicular cysts contain heterogeneous fibroblasts that can form subsets exhibiting different effects on osteoclastogenesis. The subset, which depending on the autocrine effects of EDA + FN on VEGF-A, mainly contributes to the osteoclastogenesis and bone destruction of radicular cysts. The

---

regulation of the proportion of subsets is a possible strategy for artificially interfering with osteoclastogenesis.

1 | INTRODUCTION

Heterogeneous fibroblasts have been demonstrated to exist in various connective tissues, including bone marrow, dermis (Maridas, Rendina-Ruedy, Le, & Rosen, 2018; Philippeos et al., 2018), and the stroma of viscera (Mizoguchi et al., 2018; Xie et al., 2018), in which the fibroblasts from different origins differentiate into cell subpopulations with specific gene profiles (Raz et al., 2018). These fibroblast subpopulations affect the metabolism of connective tissues by participating in angiogenesis (Du et al., 2016), hair follicle formation, the synthesis of extracellular matrix (ECM) (Driskell et al., 2013), etc. Under pathological conditions, the interactions with microenvironment components further facilitate fibroblast differentiation into distinct subsets, by which the development and fate of tumor (Ostman, 2014), fibrosis (Xie et al., 2018), inflammation (Mizoguchi et al., 2018), and wound healing (Guerrero-Juarez et al., 2019) are influenced. For instance, in lung cancers, cancer-secreted factors induced the differentiation of cancer-associated fibroblasts (CAFs) subsets (Busch et al., 2017), expressing different markers, or collagen sets (Lambrechts et al., 2018). Further, the fibroblasts surrounding microvessels became subsets with lower tumor-promoting function (Suda et al., 2016) relative to other CAFs, while in osteoarthritis, fibroblast subsets localized to the perivascular zone exhibiting proinflammatory potential (Mizoguchi et al., 2018), suggesting the functional differentiation of fibroblast subsets in lesions.

In the stroma of odontogenic cysts, osteoclastogenesis also seemed to be induced by differentiated fibroblasts in the fibrous capsules, as interacting with various components of the microenvironment. In our previous studies, the fibroblasts that were in contact with monocytes promoted osteoclastogenesis, via unregulated IL-6 and VEGF-A (Wang & Li, 2013); the interaction between epithelia and fibroblasts increased the ratio of RANKL/OPG, and hence, osteoclastogenesis was facilitated (Wang, Jiang, Sima, & Li, 2015). However, in radicular cysts, the effects of fibronectin isoforms (EDB + FN, CS1-FN, and especially EDA + FN) on the fibroblast itself influenced the expression of osteoclastogenesis-related genes, such as COX-2, IL-6, IL-17, M-CSF, IL-1α, TNF-α, RANKL, OPG, or VEGF-A (Liu & Wang, 2019; Wang, Wang, Chen, & Zhang, 2019), which led to osteoclastogenesis and bone destruction (Yang, Jiang, Wang, & Li, 2019). Odontogenic cysts are developed from inflammation or odontogenic epithelia rests, the jaw bone was destructed and formed cavities, and, microscopically, cavities are surrounded by lining epithelia and outer fibrous capsules; therefore, it is similar to other pathological conditions (Mizoguchi et al., 2018; Suda et al., 2016; Xie et al., 2018), the inflammatory cells or cytokines, abnormal ECM, epithelia or endothelia in cysts perhaps also facilitating the differentiation of fibroblast subsets to diversify their function in osteoclastogenic induction.

As the typical and most frequent odontogenic cysts characterized by jawbone destruction (Johnson, Gannon, Savage, & Batstone, 2014; Johnson, Savage, Kazoullis, & Batstone, 2013), radicular cysts are initiated by chronic inflammation and also contain inflammatory cells, cytokines, ECM, epithelia, and endothelia (Bernardi, Visioli, Nor, & Rados, 2015; Garcia, Sempere, Diago, & Bowen, 2007). Apical inflammation stimulates surrounding periodontal ligament, in which the fibroblasts proliferate and form the fibrous capsules circumventing the lining epithelia and cavity of cysts, together with accumulated collagen (Garcia et al., 2007). As the apical lesion enlarging in the jawbone, mesenchymal stroma cells (MSCs) could be recruited in the expanded capsules, participating angiogenesis, ECM synthesis, osteogenesis, and osteoclastogenesis (Yang et al., 2019).

The fibroblast subsets tend to differentiate by interacting with the pathological microenvironment, while osteoclastogenesis is induced separately, leading to different bone resorption statuses. Therefore, in this study, based on analyzing dividing fibroblasts as distinct clusters, the subset mainly contributes to osteoclastogenesis was identified and inhibited to decrease osteoclastogenesis as well as bone destruction.

2 | MATERIALS AND METHODS

2.1 | The standard for radicular cyst case selection

In Peking University School and Hospital of Stomatology, in 2018–2019, 19 patients whose radiolucent lesions surrounded the apex with necrotic pulp or filled root were selected and surgically removed, in the Department of Oral and Maxillofacial Surgery; all the lesions were diagnosed as radicular cysts, by the Department of Pathology. The period between radiographic examination and acute periapical periodontitis was no more than one year (Yang et al., 2019). As described previously (Yang et al., 2019; Zizzi et al., 2013), within at least four months before surgical excision, patients had not taken antibiotics or medication for inflammation. Every patient has written the consent to use specimens for research, and it was approved by Peking University School of Stomatology Institutional Review Board (Beijing, China; permit number: PKUSSIRB201838112). The clinical data of patients are list in Table 1.

TABLE 1 The clinical data of patients and the number of colony-forming units (CFUs)

Gender	Age	Location of lesions	Perilesional border	CFUs/1,000 cells	CFUs for further experiments
M	29	Mandible	Sclerotic	85	1
F	31	Maxillary	Unsclerotized	102	3
F	43	Maxillary	Sclerotic	107	1
F	40	Mandible	Sclerotic	94	2
M	51	Mandible	Sclerotic	101	1
F	42	Mandible	Unsclerotized	77	1
F	30	Maxillary	Sclerotic	149	3
M	38	Mandible	Unsclerotized	39	1
M	51	Mandible	Sclerotic	61	2
M	52	Mandible	Unsclerotized	43	1
M	57	Maxillary	Sclerotic	87	1
F	53	Maxillary	Sclerotic	73	1
M	25	Mandible	Unsclerotized	133	4
F	40	Maxillary	Unsclerotized	111	1
M	60	Maxillary	Unsclerotized	82	2
F	54	Mandible	Sclerotic	106	1
M	52	Maxillary	Unsclerotized	37	1
F	46	Mandible	Sclerotic	118	1
F	33	Maxillary	Unsclerotized	99	2

2.2 | Imaging and grouping the radicular cysts based on the panoramic radiograph

Digital panoramic radiographs were taken with a PM 2002 CC Prolinesystem (Planmeca OY) (filtration: 2.5 mm AlEquiv), using Kodak T-MAT G/RA dental film (Eastman Kodak). The periapical radiolucency in the jaw bone was categorized as either the perilesional sclerotic group (Zhao, Tsai, & Chang, 2014), in which the radiolucency displayed well-circumscribed sclerotic borders, or the unsclerotized group. The grouping represents different bone resorption statuses.

2.3 | Cell culture and colony-forming unit (CFU) assay

The osteoclast precursor, Raw264.7 cells, was cultured in Dulbecco's modified Eagle's medium (DMEM) (GIBCO), containing 100 g/ml streptomycin, 100 U/ml penicillin, 2 mM L-glutamine, and 10% fetal bovine serum (FBS). Cells were maintained at 37°C, in the 95% humidity, and atmosphere of 5% CO_2 (Liu & Wang, 2019; Wang et al., 2019; Yang et al., 2019).

As described previously(Liu & Wang, 2019), from the surgical specimens of 19 cases of radicular cysts, the fibroblasts were isolated from the fibrous capsules of cysts and routinely cultured in α-modified Eagle's medium (α-MEM) (GIBCO). The fibroblasts from the jawbone of 6 patients who were treated with orthognathic surgery were taken as controls (Liu & Wang, 2019; Wang et al., 2019; Yang et al., 2019). As described previously (Wang & Li, 2013), the fibroblasts were seeded into 100 mm dishes at a density of 1,000

cells/dish for 14 days, the aggregations containing no less than 50 cells were defined as a colony formation units (CFUs), and crystal violet was used to stain the cells. This CFU assay was performed at least once for each case; therefore, the biological repeat was at least 19 times for fibroblasts of cysts and 6 times for control fibroblasts.

In another set of CFU assays, the fibroblasts were seeded at a density of 100 cells/dish. On the 14th day, the aggregations containing more than 100 cells were digested by trypsin-EDTA, and the fibroblasts from each CFU were cultured in 24-well plates, as described previously (Zhang & Chan, 2010). When the confluence reached 70%, the cells were passed into dishes for further experiments. The number of CFUs in the two assays is listed in Table 1.

2.4 | Collection of conditioned medium for inducing osteoclastogenesis

When fibroblasts had grown to the confluence of 70 ~ 80% (i.e., cells have taken up 70 ~ 80% of the area of a dish) in the 60 mm or 100 mm dishes, serum-free α-MEM was used to replace the previous medium, and cells were maintained for seven days. Then, the supernatants were collected and centrifuged for 10 min at 550 g, 40% fresh α-MEM (GIBCO), and 10% FBS was added into the 50% aliquoted supernatant, to make conditioned medium (Liu & Wang, 2019; Wang et al., 2019; Yang et al., 2019). Only 39 CFUs had survived and grown sufficient fibroblasts for making the conditioned medium.

Raw 264.7 cells (1,000 cells/well) were seeded into 24-well plates, and the conditioned medium containing 12 ng/μl recombinant murine RANKL (R&D) was used for osteoclastogenic induction. Conditioned medium was refreshed at the interval of 1 day

for 10 days, and then, cells were stained with tartrate-resistant acid phosphatase (TRAP) kit (Sigma). Cells containing no less than three nuclei and stained with TRAP (Trap + MNCs) were defined as osteoclast-like cells (Liu & Wang, 2019; Wang et al., 2019; Yang et al., 2019). The conditioned medium of each CFU was added into four wells, for inducing the Trap + MNCs.

2.5 | Modulation of the conditioned medium and knockout of the EDA exon

As described in our previous studies (Liu & Wang, 2019; Wang et al., 2019; Yang et al., 2019), IST-9 antibody (Abcam) was added into the medium of fibroblasts to specifically block the effects of EDA + FN on the fibroblasts themselves, and bevacizumab (Genentech Inc.) was added to the conditioned medium for blocking the interaction between VEGF-A and preosteoclasts. The experiments of blocking by IST-9 or bevacizumab were repeated at least three times for each group (Figure 3d).

Using the same protocol that was used in previous studies (Liu & Wang, 2019; Wang et al., 2019; Yang et al., 2019), once reaching the confluence of 70%–90%, medium was replaced with serum-free one and maintained for six hours, plasmids containing sequences of single-guide (sg) RNAs which recognize the DNA flanking EDA exon co-transfected with Lipofectamine 2000, as described in manufacturer's protocol (Life Technologies). Primer sequences and sgRNAs were identical to that described in our previous study (Yang et al., 2019) (Table 2).

2.6 | Critical-sized alveolar defect model and injection of fibroblasts

Eight-week-old male Sprague Dawley rats from the Laboratory Animal Center of Tongji University were used in this study, following the International Guiding Principles for Animal Research (1985). The experimental protocol was approved by the Laboratory Animal Center of Tongji University (No. [2019]-DW-017).

Before surgery, the rats were acclimatized to animal housing facility cages, fed standard laboratory diet, and were housed at ambient temperature and humidity. As described previously (Boda et al., 2019; Xu & Wang, 2017), surgery was performed in rats using sodium pentobarbital for general anesthesia. The socket of the removed M1 tooth was enlarged to a critical-sized defect of 2 mm diameter and 2 mm depth, on both sides in the maxillary bone, by 2 mm diameter under saline irrigation. The gum was stitched to cover the defects (Liang et al., 2016).

Fibroblasts were digested using trypsin, were washed twice with phosphate-buffered saline (PBS), and were resuspended at a concentration of 1×10^7 cells/ml in PBS. Then, after 1 day, in the experimental rats ($n = 6$), 1×10^6 untreated, or EDA knockout fibroblasts were injected into the submucosa surrounding the left or right bone defects, respectively. On the 7th day, the animals were sacrificed, and the tissues were collected. In the left maxillary bone of another 6 rats, the untreated defects were taken as controls.

2.7 | Immunohistochemical (IHC) investigation of the specimens

Radicular cyst specimens were formalin-fixed, paraffin-embedded, and sectioned into 4-μm-thick slices which were then stained with antibodies, including IST-9, anti-VEGF-A, and anti-CD34 antibodies (Abcam Ltd.), at 4°C overnight, for the purpose of investigating EDA + FN, VEGF-A, and endothelia. The negative control was incubated with PBS. Subsequently, at 37°C, biotinylated secondary antibody (1:200) was used to incubate slices, for 1 hr. Immunocomplexes were visualized with diaminobenzidine (Zhongshan Golden Bridge Biological Technology Co., Ltd.).

As described previously (Liu & Wang, 2019; Wang et al., 2019; Yang et al., 2019), EDA + FN and VEGF-A staining were investigated by microscope (Olympus) and quantified with Image-Pro Plus ver. 6.0 software (Media Cybernetics). The optical density was calibrated as previously described (Liu & Wang, 2019; Wang et al., 2019; Yang et al., 2019), by which the groups of high or low expression were demarcated; CD34 + vascular endothelia were identified as microvessels, and the groups of high or low density were demarcated according to previous standard (Yang et al., 2019), in which the area (μm^2) of microvessels within the depth of 500 μm from the lining epithelium were calculated, in randomly selected at least 3 high-power fields (hpf: 400× magnification).

2.8 | RNA extraction, reverse transcription, and PCR amplification

RNA was extracted by TRIzol Reagent (Life Technologies) from cells, and 2 μg total RNA was reverse-transcribed into cDNA by superscript first-strand synthesis kit (Life Technologies). Real-time PCR was conducted with 20 μl mixture, with a LightCycler real-time PCR system (Roche Diagnostics Ltd), according to the following parameters: 95°C for 10 min, 40 cycles of annealing/extension at 60°C (1 min/cycle), and then denaturation at 95°C for 15 s. FN isoforms and osteoclastogenesis-related genes were assessed. Human β-actin was used to normalize relative expression. For each gene of every sample, the real-time PCR was performed at least four times. The primers are listed in Table 3.

2.9 | Statistics

Quantitative data were expressed by means ± standard deviation (*SD*), and the differences among three or more groups were assessed using one-way ANOVA with repeated measures followed by the LSD or Tamhane's multiple comparison test. The differences between two groups were evaluated using Student's *t*-test. As described previously (Kawagishi-Hotta et al., 2017), characteristics of each CFU were evaluated by principal component analysis (PCA), using the assessed FN isoforms and osteoclastogenesis-related genes. Each measured value was normalized to use for PCA. Components with an eigenvalue ≥1.0

TABLE 2 Sequences of CRISPR sgRNA and confirming primers

Name	sgRNA sequence (5'–3')	PAM sequences (5'–3')	DSB site in fibronectin (FN) genome (ref|NC_018913.2|)
sgRNA up-stream-F	GTTACAGACATTGATCGCCCTAA	AGG	216251686
sgRNA up-stream-R	AACTTAGGGCGATCAATGTCTGT		
sgRNA down-stream-F	GTTCTGATTGGAACCCAGTCCAC	AGG	216251434
sgRNA down-stream-R	AACGTGGA CTGGGTTCCAATCAG		
	Primers	**Product containing EDA**	**Product without EDA**
Primer-down	atagtgggttaattggact	675 bp	415 bp
Primer-up	agggtaatcacagggag		

TABLE 3 The primers used for real-time PCR

Osteoclastogenesis-related genes	Forward primers (5'–3')	Reverse primers (5'–3')	Sites of amplification
EDA + FN (NM_212482)	AggACTggCATTCACTgATgTg	gTCACCCTgTACCTggAAACTTg	5447–5533
EDB + FN (NM_212482)	ggTggACCCCgCTAAACTC	ACCTTCTCCTgCCgCAACTA	4128–4190
CS1-FN (NM_212482)	TTCCCCAACTggTAACCCTT	TTTAAAgCCTgATTCAgACTCg	6520–7229
	Forward primers (5'–3')	**Reverse primers (5'–3')**	**Gene ID**
IL–6	AACCTgAACCTTCCAAAgATgg	TCTggCTTgTTCCTCACTACT	NM_000600.4
IL–1α	AgATgCCTgAgATACCCAAAACC	CCAAgCACACCCAgTAgTCT	NM_000575.4
TNF-α	gAggCCAAgCCCTggTATg	CgggCCgATTgATCTCAgC	NM_000594.3
M-CSF	AgACCTCgTgCCAAATTACATT	AggTgTCTCATAgAAAgTTCggA	NM_000757.5
VEGF-A	TTATgCggATCAAACCTCACC	gAAgCTCATCTCTCCTATgTgC	NM_001171623.1
IL–17	CCggAATACCAATACCAATCCC	AggTggATCggTTgTAgTAATCT	NM_002190.2
COX–2	CCAgTATAAgTgCgATTgTACCC	TCAAAAATTCCggTgTTgAgCA	NM_000963.3
OPG	CACAAATTgCAgTgTCTTTggTC	TCTgCgTTTACTTTggTgCCA	NM_002546.3
RANKL	AgATCgCTCCTCCATgTACCA	gCCTTgCCTgTATCACAAACTT	NM_003839.3
β-actin	CATgTACggTTgCTATCCAggC	CTCCTTAATgTCAcgCACgAT	NM_001101.3

were taken as principal components (PCs), in automated population separator (APS) view, as a linear combination of parameters with distinct statistical weights, different PC represented each axis of a plot. On this basis, selected clusters were compared with each other to find significantly different bins in search of cellular subsets (Henriques et al., 2016). According to the EDA + FN and VEGF-A staining, as well as CD34+ microvessel areas, the clinicopathological samples were divided into groups and evaluated with chi-square tests. Statistical significance was set at $p < .05$. SPSS version 19.0 software (SPSS Inc.) was used to perform the statistical analyses. Each experiment was performed in triplicate.

3 | RESULTS

3.1 | Colony formation among groups of radicular cysts based on radiographic investigation

According to the pathological diagnosis, panoramic radiographs of radicular cysts were collected, and all lesions exhibited periapical radiolucency in the jawbone. The lesions of 10/19 cases displayed well-circumscribed sclerotic borders, as reported previously (Zhao et al., 2014); the lesions (9/19) appearing with unsclerotized borders resembled that of odontogenic keratocysts (OKC) (Morgan, 2011) (Figure 1a). Based on radiographic investigation, the radicular cysts were divided into perilesional sclerotic and unsclerotized groups, representing different statuses of bone resorption.

The number of colony-forming units (CFUs) developed from fibroblasts in the perilesional sclerotic group (n = 10, 98.1000 ± 23.3557) was approximately the same as that of unsclerotized group (n = 9, 80.3333 ± 32.5337, p = .0.1730); similarly, the CFUs developed from the fibroblasts of control group (n = 6, 101.5000 ± 16.3376) were also similar to that of the perilesional sclerotic (p = .8127) and unsclerotized groups (p = .1577) (Figure 1b). Each aggregation of CFUs contained more than 50 cells, and the cells displayed well spread, spindle-shaped, and elongated fibroblast-like appearance, as same as the fibroblasts from other odontogenic cyst (Wang & Li, 2013) (Figure 1c).

In another set of CFU assays, there were 14 CFUs from the perilesional sclerotic group, 16 CFUs from the unsclerotized group, and 9 CFUs from the control group that survived for the subsequent osteoclastogenic induction assay.
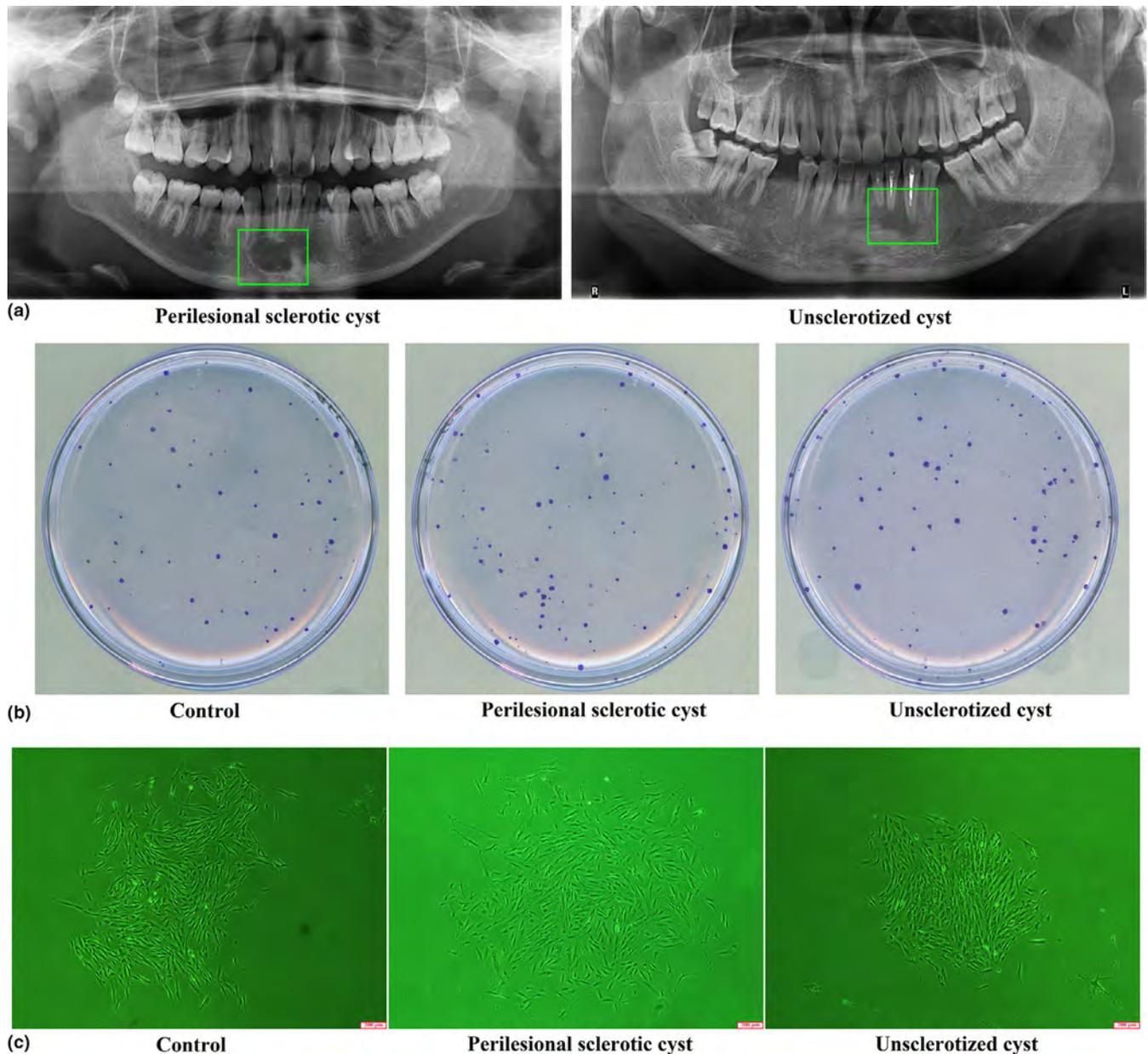
FIGURE 1 (a) The panoramic radiograph of the perilesional sclerotic and unsclerotized radicular cysts. (b) The colony formation units (CFUs) developed in dishes from 1,000 cells isolated from the control, perilesional sclerotic, and unsclerotized groups. (c) The fibroblast aggregations of CFUs from control, perilesional sclerotic, and unsclerotized groups (with original magnification ×40, scale bar: 200 μm)

3.2 | Comparing the osteoclastogenic induction and gene expression of CFUs among groups of radicular cyst

The fibroblasts of all CFUs could induce the formation of Trap + MNCs. CFUs from unsclerotized cysts induced significantly more Trap + MNCs ($n = 16$, 15.5313 ± 7.0076/well) than the CFUs from perilesional sclerotic cysts ($n = 14$, 7.5536 ± 5.8934/well, $p = .0008$), as well as controls ($n = 9$, 4.8889 ± 3.0774/well, $p = .0001$); however, the difference between the latter two groups was insignificant ($p = .2995$; Figure 2a,b). The expression of osteoclastogenesis-related genes in the CFUs was also consistent with their effects on Trap + MNCs formation. For example, the expression of EDA + FN, COX-2, IL-6, IL-1α,

TNF-α, VEGF-A, and RANKL in the fibroblasts of CFUs from unsclerotized cysts was highest among the three groups, and the OPG was the lowest; hence, in the fibroblasts from unsclerotized cysts, the ratio of RANKL/OPG, which reflecting the osteoclastogenic induction (de Moraes, de Lucena, de Azevedo, Queiroz, & Costa Ade, 2011), was also highest among the three groups (Figure 2c; Table 4).

3.3 | Cluster analysis of all the CFUs based on principal component analysis

Principal component analysis (PCA) allowed analysis of whole profiles of assessed osteoclastogenesis-related genes in fibroblasts
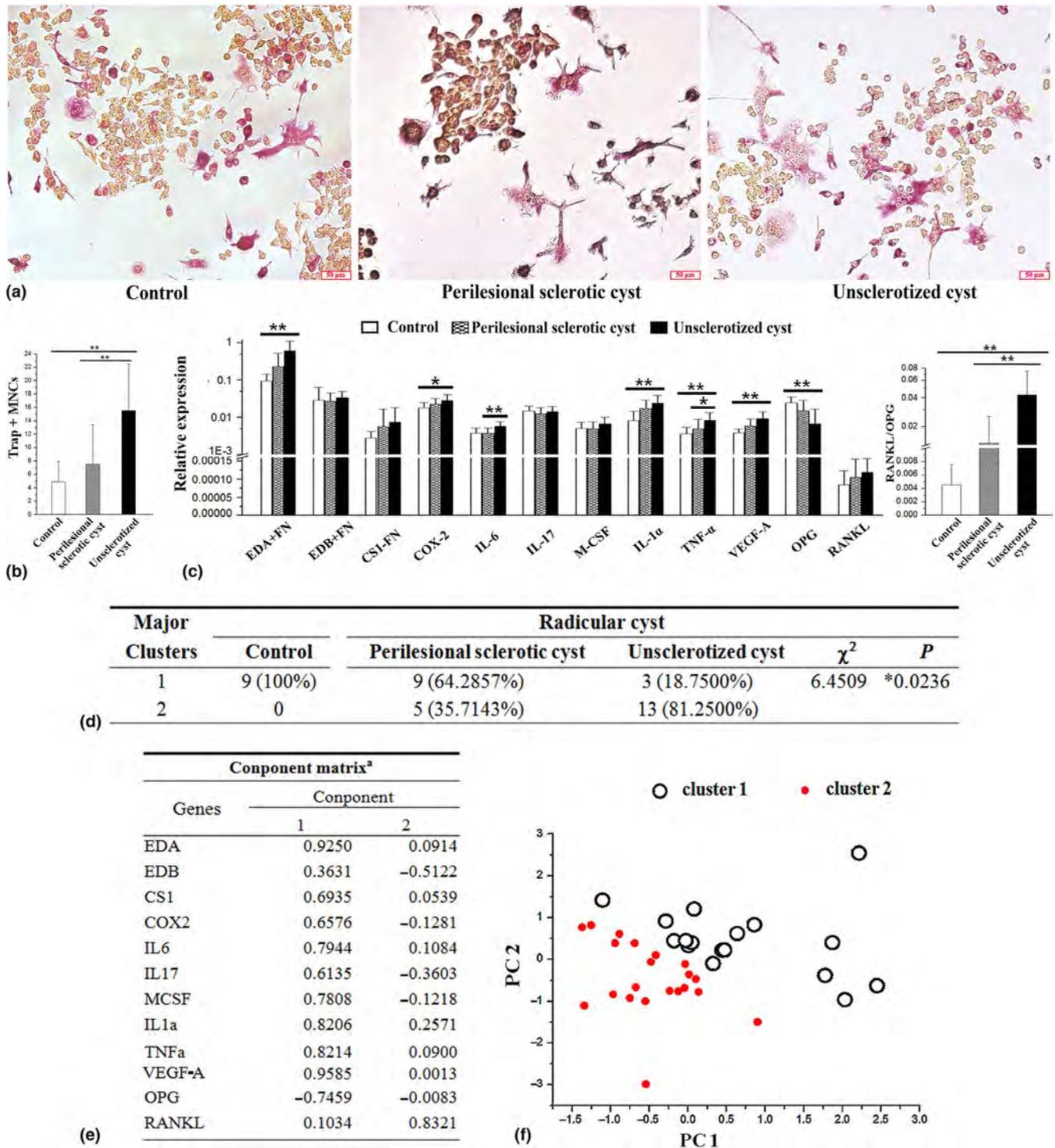
FIGURE 2 (a) The Trap + MNCs induced by fibroblast CFUs isolated from the groups of controls, perilesional sclerotic, and unsclerotized cysts (with original magnification ×200, scale bar: 50 μm). (b) The comparison of Trap + MNCs induced by fibroblast CFUs among the three groups. (c) The relative expression of osteoclastogenesis-related genes among the three groups, as well as the ratio of RANKL/OPG. (d) To compare the percentage of CFUs in each clusters among the three groups, by the chi-square test. (e) The factor loading of osteoclastogenesis-related genes on the PC1 and PC2, and the genes are displayed in a decreasing order of their factor loading on PC1. (f) Each circle or spot represents a median position of each CFU in the coordinate system of PC1 versus PC2.(Black circle: CFUs of Cluster 1; Red spot: CFUs of Cluster 2.)

from each CFU (Henriques et al., 2016). Principal components (PCs) in which the eigenvalue ≥1 were calculated to examine the variations in fibroblasts of CFUs, as described previously (Kawagishi-Hotta et al., 2017). In the present study, PC1 and PC2 accounted for 52.9328% and 10.1094% of the variance among CFUs, respectively (Table 5), and the factor loading of VEGF-A

TABLE 4 Relative expression of genes in the fibroblasts from control, perilesional sclerotic, and unsclerotized cyst

Osteoclastogenesis-related genes	Relative expression			p		
	1 (Control)	2 (perilesional sclerotic cyst)	3 (unsclerotized cyst)	1/2	1/3	2/3
EDA + FN	0.0941 ± 0.0492	0.2290 ± 0.3021	0.6042 ± 0.5036	.3276	.0032**	.0558
EDB + FN	0.0287 ± 0.0360	0.0274 ± 0.0172	0.0338 ± 0.0162	.8892	.5895	.4384
CS1-FN	0.0028 ± 0.0015	0.0056 ± 0.0112	0.0075 ± 0.0110	.5078	.5947	.5947
COX2	0.0183 ± 0.0068	0.0226 ± 0.0093	0.0283 ± 0.0119	.3221	.0222*	.1301
IL6	0.0038 ± 0.0014	0.0037 ± 0.0013	0.0057 ± 0.0019	.9983	.0059	.0020**
IL17	0.0149 ± 0.0052	0.0126 ± 0.0060	0.0141 ± 0.0056	.3343	.7151	.4739
M-CSF	0.0051 ± 0.0023	0.0050 ± 0.0026	0.0068 ± 0.0033	.9759	.1603	.1040
IL–1α	0.0082 ± 0.0062	0.0174 ± 0.0112	0.0238 ± 0.0155	.0922	.0048**	.1683
TNF-α	0.0036 ± 0.0019	0.0050 ± 0.0040	0.0084 ± 0.0049	.4191	.0067**	.0260*
VEGF-A	0.0038 ± 0.0011	0.0058 ± 0.0033	0.0093 ± 0.0048	.1418	.0001**	.0740
OPG	0.0244 ± 0.0108	0.0151 ± 0.0134	0.0067 ± 0.0098	.0646	.0007**	.0533
RANKL	8.5389E–5 ± 3.8610E–5	1.055E–4 ± 5.0019E–5	1.1930E–4 ± 3.7561E–5	.2798	.0648	.3803

*$p < .05$.
**$p < .01$.

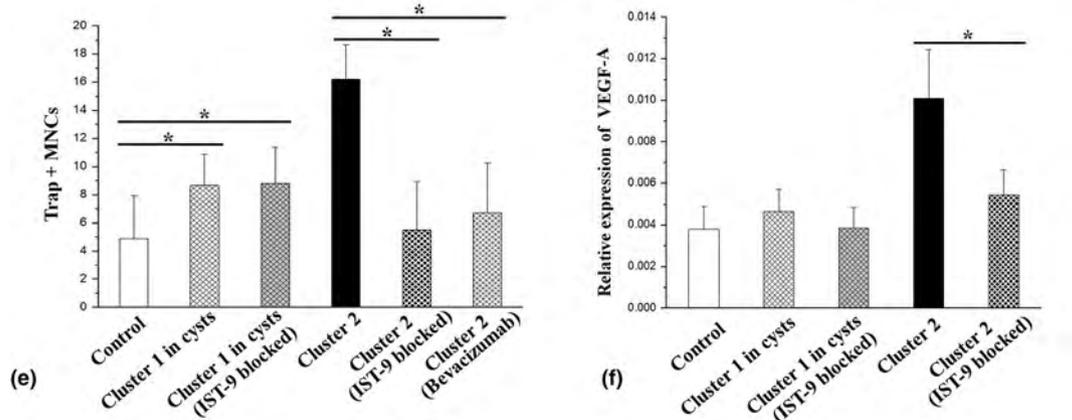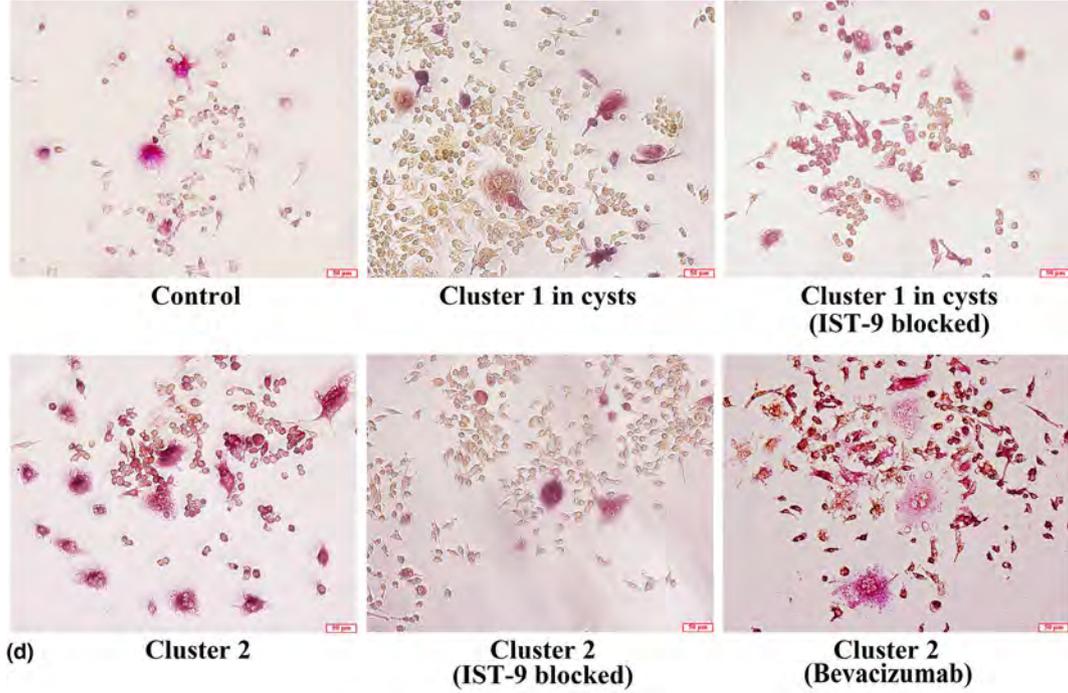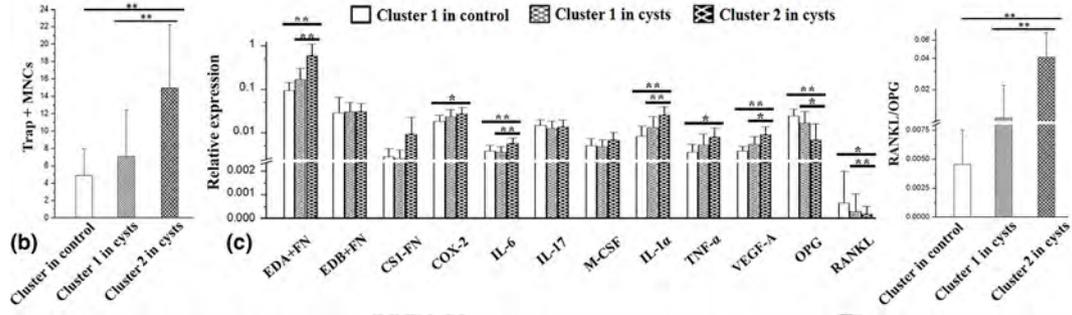**TABLE 5** The total variance explained by the components

Component	Initial Eigenvalues			Extraction Sums of Squared loadings		
	Total	% of Variance	Cumulative %	Total	% of Variance	Cumulative %
1	6.3519	52.9328	52.9328	6.3519	52.9328	52.9328
2	1.2131	10.1094	63.0422	1.2131	10.1094	63.0422
3	0.9096	7.5803	70.6225			
4	0.7724	6.4369	77.0594			
5	0.7425	6.1873	83.2467			
6	0.5955	4.9623	88.2090			
7	0.4160	3.4664	91.6754			
8	0.3774	3.1453	94.8207			
9	0.2874	2.3952	97.2159			
10	0.1655	1.3795	98.5954			
11	0.1330	1.1083	99.7037			
12	0.0356	0.2963	100.0000			

and EDA + FN on principal components 1 (PC1) was higher than that of other genes.(Figure 2e).

According to the median position of individual CFUs in the co-ordinate analysis of PC1 versus PC2, the fibroblasts from the CFUs could be divided into two clusters (Cluster 1 and 2), representing distinct profiles of assessed osteoclastogenesis-related genes. All the CFUs isolated from the control group were in Cluster 1; and a majority of CFUs from perilesional sclerotic cysts belonged to Cluster 1. The majority of Cluster 2 were derived from unsclerotized cysts, which developed significantly higher proportion of Cluster 2 than perilesional sclerotic cysts (χ^2 = 6.4509, p = .0236) (Figure 2d).

FIGURE 3 (a) The Trap + MNCs induced by fibroblasts belonging to the groups of Cluster 1 in cyst, Cluster 2 in cyst and Cluster in control (with original magnification ×200, scale bar: 50 μm). (b) The comparison of Trap + MNCs induced by fibroblast among the three groups. (c) The comparison of relative expression of osteoclastogenic genes among the three groups, as well as the ratio of RANKL/OPG. (d) The Trap + MNCs induced by untreated fibroblasts of controls, Cluster 1 in cyst and Cluster 2, as well as their counterparts treated by IST-9 and bevacizumab, respectively (with original magnification × 200, scale bar: 50 μm). (e) The comparison of Trap + MNCs induced by the untreated fibroblasts, and the counterparts treated by IST-9 or bevacizumab. (f) The relative expression of VEGF-A in the controls, untreated fibroblasts, and their counterparts treated by IST-9 or bevacizumab

(a) Cluster 1 in control — Cluster 1 in cysts — Cluster 2 in cysts

(b) (c) □ Cluster 1 in control ▨ Cluster 1 in cysts ▧ Cluster 2 in cysts

(d) Control — Cluster 1 in cysts — Cluster 1 in cysts (IST-9 blocked)

Cluster 2 — Cluster 2 (IST-9 blocked) — Cluster 2 (Bevacizumab)

(e) (f)

According to the Clusters to which the CFUs belonged, as well as their derivations, CFUs were identified as three groups: Cluster 1 in cyst and Cluster 2 in cyst, as well as the Cluster in control, and for the control, all CFUs belonged to Cluster 1.

3.4 | Comparing the osteoclastogenic induction and gene expression among groups of Clusters

The number of Trap + MNCs induced by fibroblasts of Cluster in control ($n = 9$, 4.8889 ± 3.0774/well, $p < .0001$), as well as by fibroblasts of Cluster 1 in cyst ($n = 12$, 7.0652 ± 5.4053/well, $p = .0059$), was significantly smaller than that induced by the fibroblasts of Cluster 2 in cyst ($n = 18$, 14.9722 ± 7.2416/well); the differences between the former two groups were insignificant ($p = .5942$) (Figure 3a,b). The osteoclastogenesis-related gene expression among groups was also consistent with the osteoclastogenic effects. In the fibroblasts belonging to Cluster 2 in cysts, the expression of EDA + FN, COX-2, IL-6, IL-1α, TNF-α, VEGF-A, and RANKL and the ratio of RANKL/OPG were highest, and the OPG expression was lowest among the three groups (Figure 3c; Table 6).

3.5 | The effects of blocking EDA + FN or VEGF-A on osteoclastogenesis among groups of Clusters

As the CFUs were mixed according to their cluster groups, monoclonal antibody IST-9 was used to block the autocrine effect of EDA + FN on fibroblast itself, and the bevacizumab blocked the interaction between VEGF-A and preosteoclasts in the conditioned medium, as described in our previous studies (Wang et al., 2019; Yang et al., 2019).

The number of Trap + MNCs induced by untreated fibroblasts of Cluster 1 in cyst ($n = 4$, 8.6875 ± 2.2209/well, $p = .0427$), as well as those induced by IST-9 blocked Cluster 1 in cyst ($n = 4$, 8.8125 ± 2.6011/well, $p = .0369$), was significantly larger than those induced by control fibroblasts ($n = 9$, 4.8889 ± 3.0774/well), but there were insignificant differences between the former two groups ($p = .9523$; Figure 3d,e). Consistently, the expression of VEGF-A in Cluster 1 in cysts was also unaffected when the fibroblasts were treated with IST-9 (0.0046 ± 0.0009 vs. 0.0039 ± 0.0010, $p = .3962$; Figure 3d,f), suggesting the independence on EDA + FN and VEGF-A.

However, the number of Trap + MNCs induced by untreated fibroblasts of Cluster 2 ($n = 3$, 16.2500 ± 2.4109/well) was significantly decreased when the fibroblasts were treated with IST-9 ($n = 3$, 5.5000 ± 3.4369/well, $p = .0002$; Figure 3d,e), which was also accompanied by significant declined VEGF-A expression (0.0101 ± 0.0024 vs. 0.0022 ± 0.0012, $p < .0001$; Figure 3d,f). Consistently, the conditioned medium containing bevacizumab also significantly decreased Trap + MNC formation ($n = 3$, 6.7500 ± 3.5000/well, $p = .0007$), in contrast with what was observed in untreated fibroblasts (Figure 3d,e), suggesting the autocrine effect of EDA + FN on VEGF-A, as described previously (Wang et al., 2019; Yang et al., 2019).

3.6 | Retrospective analysis of EDA + FN and VEGF-A expression and the density of microvessels via clinicopathological data

Clinicopathological data of radicular cysts were analyzed again by investigating EDA + FN and VEGF-A staining, as well as the CD34 marked microvessels, in the fibrous capsules of radicular

TABLE 6 Relative expression of genes among the fibroblasts of cluster groups

| Osteoclastogenesis-related genes	Relative expression			P		
	1 (Cluster in control)	2 (Cluster 1 in cyst)	3 (Cluster 2 in cyst)	1/2	1/3	2/3
EDA + FN	0.0941 ± 0.0492	0.1681 ± 0.1409	0.6031 ± 0.5123	.3025	.0018**	.0079**
EDB + FN	0.0287 ± 0.0360	0.0305 ± 0.0188	0.0310 ± 0.0157	.8593	.8056	.9523
CS1-FN	0.0028 ± 0.0015	0.0025 ± 0.0015	0.0093 ± 0.0135	.9482	.0944	.0579
COX2	0.0183 ± 0.0068	0.0232 ± 0.0112	0.0272 ± 0.0109	.2778	.0391*	.3049
IL6	0.0038 ± 0.0014	0.0036 ± 0.0012	0.0056 ± 0.0019	.8017	.0071**	.0015**
IL17	0.0149 ± 0.0052	0.0125 ± 0.0060	0.0139 ± 0.0056	.3410	.6667	.5096
M-CSF	0.0051 ± 0.0023	0.0048 ± 0.0020	0.0067 ± 0.0034	.8186	.1547	.0702
IL–1α	0.0082 ± 0.0062	0.0132 ± 0.0102	0.0259 ± 0.0138	.3272	.0006**	.0054**
TNF-α	0.0036 ± 0.0019	0.0052 ± 0.0042	0.0079 ± 0.0049	.3807	.0155*	.0917
VEGF-A	0.0038 ± 0.0011	0.0054 ± 0.0028	0.0091 ± 0.0047	.2498	.0005**	.0281*
OPG	0.0244 ± 0.0108	0.0166 ± 0.0141	0.0068 ± 0.0092	.1150	.0005**	.0284*
RANKL	6.5605E−4 ± 1.7100E-3	3.0342E−4 ± 7.3850E-4	2.0423E−4 ± 3.1648E-4	.9218	.0077*	.0052**

*$p < .05$.

**$p < .01$.
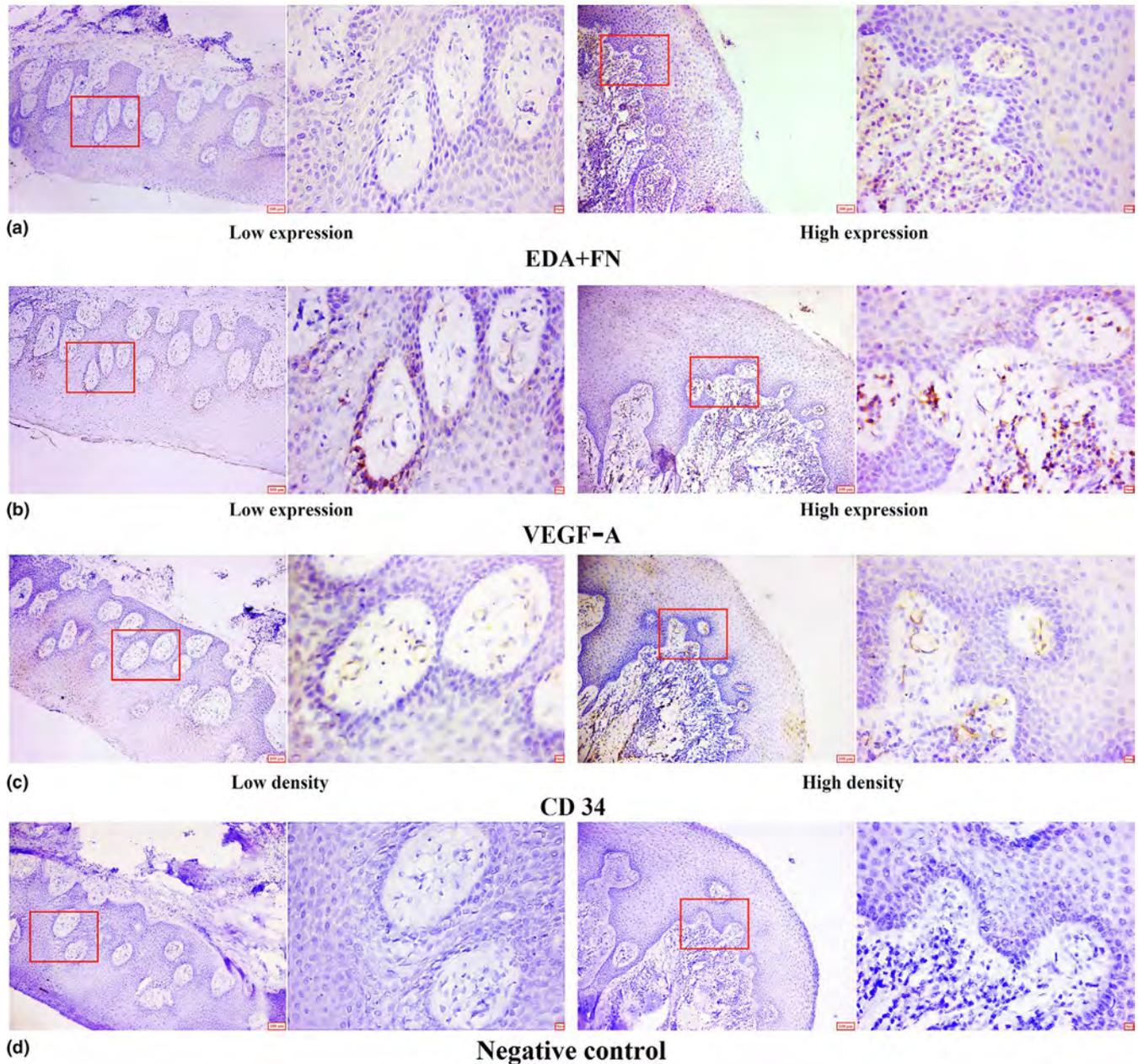
FIGURE 4 (a) The evaluation of the EDA + FN staining in the fibrous capsules of perilesional sclerotic and unsclerotized radicular cysts. (b) The evaluation of the VEGF-A staining in the fibrous capsules of radicular cysts. (c) The evaluation of microvessels according to areas surrounded by CD34 positive endothelia. (d) The negative staining control (with original magnification ×100, scale bar: 100 μm; local magnification ×400, scale bar: 10 μm)

cysts. Consistent with our previous studies (Wang et al., 2019; Yang et al., 2019), the staining for EDA + FN and VEGF-A exhibited a diffuse pattern in the fibrous capsule, and the microvessel areas were surrounded by CD34-stained vascular endothelial cells (Figure 4a-d). In the unsclerotized cysts, most of the samples revealed high expression of EDA + FN (χ^2 = 6.7388, p = .0198) and VEGF-A (χ^2 = 6.3427, p = .0230), which was in contrast with perilesional sclerotic cysts. However, the differences in the density of microvessels, as marked by CD34, exhibited little significance between the two groups (χ^2 = 2.7732, p = .1698) (Table 7).

3.7 | The interference of osteoclastogenesis in vivo by injecting modified fibroblast subset

EDA exon was knocked out in the genome of fibroblasts of Cluster 2, as described previously (Liu & Wang, 2019; Wang et al., 2019; Yang et al., 2019). The PCR products of EDA knockout cells generated a band containing EDA exon (675 bp) and another band without EDA exon (415 bp), as confirmed by DNA sequencing, suggesting a partly modified fibroblast subset (Figure 5a,b). It was consistent with our previous studies (Lv et al., 2017; Wang, Yang, et al., 2015); in the EDA knockout cells, the decreased protein level of

TABLE 7 Correlation between pathological characteristics and cyst grouping

Parameters	Perilesional sclerotic cyst	Unsclerotized cyst	χ^2 value	*p*-value
EDA + FN expression（IOD/μm^2）				
≤50	7 (70%)	1 (11.1%)	6.7388	.0198*
>50	3 (30%)	8(88.9%)		
VEGF-A expression				
≤2.2	8 (80%)	2 (22.2%)	6.3427	.0230*
>2.2	2 (20%)	7 (77.8%)		
Microvessel density				
≤2,400 μm^2	6 (60%)	2 (22.2%)	2.7732	.1698
>2,400 μm^2	4 (40%)	7 (77.8%)		

*$p < .05$.

EDA + FN was accompanied by almost unchanged total FN levels, and the VEGF-A also decreased slightly (Figure 5c).

According to previous studies (Liang et al., 2016; Traxler et al., 2016), the untreated and partly modified fibroblasts of Cluster 2 were injected into the submucosa surrounding the bone defects in the animal models, respectively. At the 7th day, osteoclasts appeared at the interface between bone and connective tissue, in the zone surrounding bone defects (Figure 5e). The animal model injected with modified fibroblasts developed significantly fewer osteoclasts (n = 6, 6.5000 ± 2.6300), in contrast with the animal injected with untreated fibroblasts (n = 6, 10.6667 ± 3.1972, p = .0481), which was similar to the animals whose bone defects were untreated (n = 6, 10.5000 ± 3.5940), suggesting that the osteoclastogenesis could be interfered by changing the proportions of fibroblast subsets (Figure 5d,e).

4 | DISCUSSION

The lesions of radicular cysts always form the radiolucent areas in the jawbone; some cases exhibited perilesional sclerotic radiolucency (Zhao et al., 2014), and most patients with this type lack acute clinical symptoms, such as pain and swelling; however, almost all the patients without perilesional sclerosis exhibit acute symptoms (Sukegawa et al., 2019). In the unsclerotized cysts, the inconspicuous lesion border resembles that of some odontogenic keratocysts (OKC), which is characterized by local aggressiveness of the jawbone (Wang, Jiang, et al., 2015; Wang & Li, 2013). Therefore, the radicular cysts with perilesional sclerotic radiolucency (perilesional sclerotic group) represented a group with lower levels of bone destruction, while the cysts lacking perilesional sclerosis (unsclerotized group) showed active bone resorption. The spindle-like morphology of fibroblasts reflected the derivation from stroma (Wang & Li, 2013), but the efficiencies of colony formation indicated little difference among the perilesional sclerotic, unsclerotized, and control groups, suggesting insignificant associations between the activity of bone resorption and fibroblast proliferation.

The bone resorption was consistent with the osteoclastogenic induction of fibroblasts, since the colony formation units (CFUs) of fibroblast isolated from the unsclerotized group induced significantly more Trap + MNCs than CFUs from other groups; correspondingly, in the former, the expression of the osteoclastogenesis-related genes COX-2, IL-6, IL-1α, TNF-α, VEGF-A and the ratio of RANKL/OPG were also highest among the three groups; EDA + FN was also highest in this group, which is a characteristic component of chronic inflammation (Kumra & Reinhardt, 2016; Shinde et al., 2015) and facilitates osteoclastogenesis by increasing the levels of other cytokines (Liu & Wang, 2019). The panel of osteoclastogenesis-related genes was expressed individually in each fibroblast colony, perhaps making up distinctive subsets with similar gene expression profiles, by which bone resorption tends to be affected. To verify those observations, PCA was performed, and two principal components (PC1 & PC2) were used; although the minority of variance in colonies could partially be attributed to genes that were not measured in this study, PC1 and PC2 still accounted for the majority of variance (63.04%), and hence, all fibroblast CFUs were assigned to one of two clusters (1 and 2) using cluster analysis, as described previously (Henriques et al., 2016).

The majority of CFUs from the perilesional sclerotic group (64.29%) and all colonies from control group (100%) belonged to Cluster 1; this result was consistent with their relatively lower function of inducing osteoclastogenesis. In contrast, most CFUs (81.25%) from the unsclerotized group belonged to Cluster 2, and the CFUs of Cluster 2 induced the production of significantly more Trap + MNCs than the CFUs of other groups (Cluster from control &Cluster 1 from cysts), suggesting an association between distinctive fibroblast subsets and the activity of bone resorption. On the other hand, among the three groups (Cluster from control, Cluster 1 from cysts, and Cluster 2), the differentially expressed osteoclastogenesis-related genes were COX-2, IL-6, IL-1α, TNF-α, VEGF-A, RANKL/OPG, and EDA + FN, which is similar to the profile of genes in the groups of radicular cysts (perilesional sclerotic, unsclerotized, and control), as mentioned above. This result further suggested that in radicular cysts, the activity of bone resorption was influenced by the proportion of different fibroblast subsets, which were categorized here as
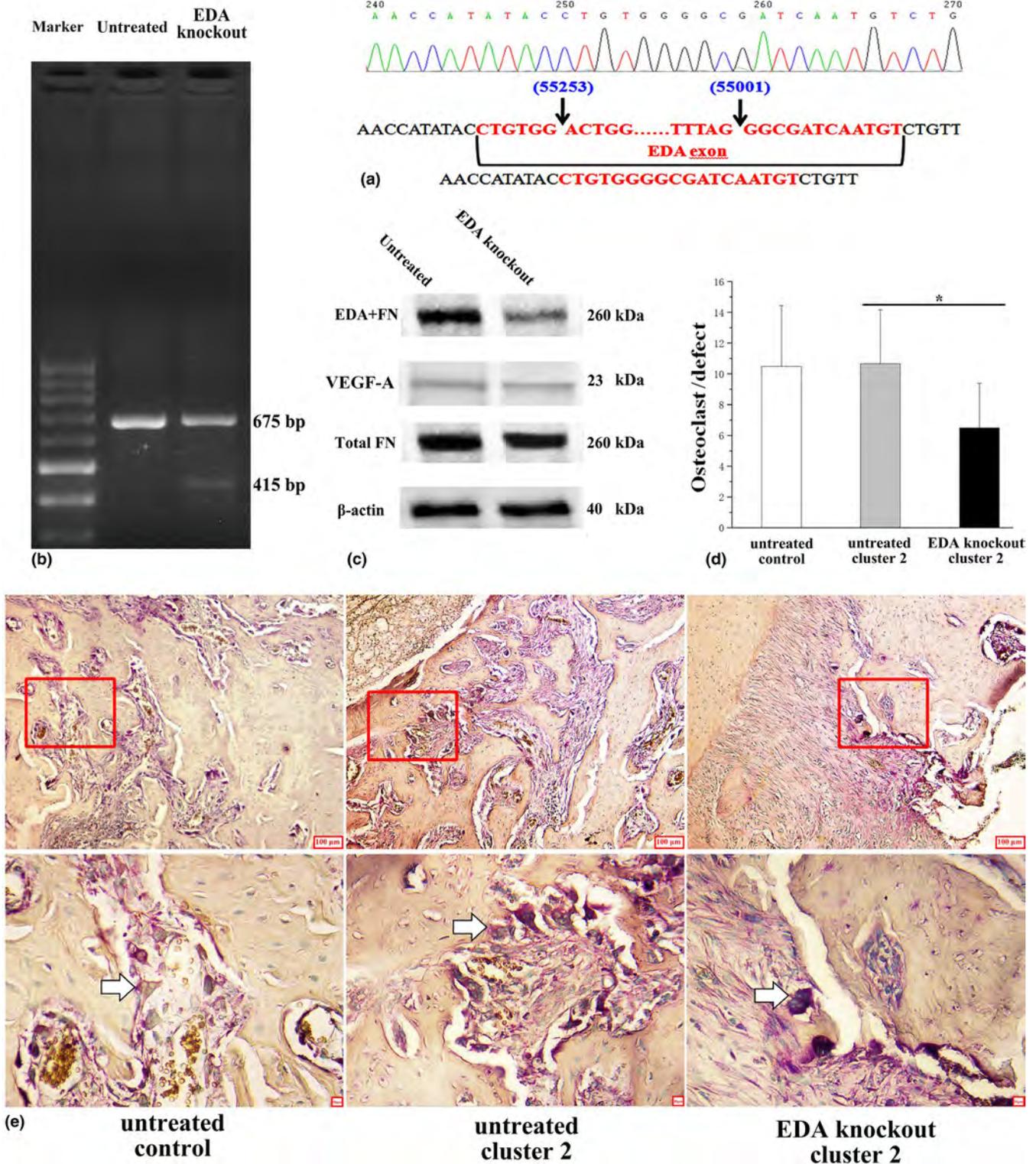
FIGURE 5 (a) Sequencing of the PCR products (415 bp) of genome without EDA exon. (b) The bands of PCR products from EDA knockout cells (415 bp), as well as the untreated cells (415 bp). (c) The protein level of VEGF-A, EDA + FN, and total FN, in EDA knockout and untreated cells, by Western blot. (d) The comparison of osteoclasts developed in the bone defects of animal models, among the groups of untreated controls, animal injected with untreated or EDA knockout fibroblasts of Cluster 2. (e) The osteoclasts appeared at the interface between bone and connective tissue, in the zone surrounding bone defects, among the three groups (with original magnification ×100, scale bar: 100 μm; local magnification ×400, scale bar: 10 μm)

Cluster 1 and 2 (Busch et al., 2017). Therefore, Cluster 2 may be important in osteoclastogenesis, and the ablation of this subset may have therapeutic applications in bone destruction (Lv et al., 2017; Philippeos et al., 2018).

Consistent with our previous studies, the autocrine effect of EDA + FN on fibroblast itself mediated gene expression (Liu & Wang, 2019), in which VEGF-A was the most important one inducing osteoclastogenesis and bone destruction (Wang et al., 2019; Yang et al., 2019). In this study, the factor loading of VEGF-A and EDA + FN was also higher than other genes in principal component 1 (PC1), which accounted for half of the variance in the CFUs (52.93%), suggesting their importance in osteoclastogenesis. Blocking EDA + FN by treatment with IST-9 in Cluster 1 did not alter VEGF-A expression or Trap + MNC formation, suggesting that the osteoclastogenesis induced by Cluster 1 was independent of EDA + FN and VEGF-A. However, EDA + FN and VEGF-A seemed crucial to the osteoclastogenic induction of Cluster 2. This was illustrated by the blockage of EDA + FN and VEGF-A, by which Trap + MNCs decreased to similar levels, and the downregulation of VEGF-A in EDA + FN blocked fibroblasts was also consistent with what we observed in previous studies (Wang et al., 2019; Yang et al., 2019), which suggests that in radicular cysts, the fibroblasts identified as Cluster 2 tended to be responsible for active bone resorption.

Through retrospective analysis of clinicopathological data, the fibrous capsule of unsclerotized cysts exhibited intense EDA + FN and VEGF-A staining, which was in contrast with perilesional sclerotic cysts, and suggested the fibroblast subset in Cluster 2 were dominant in lesions with active bone destruction. These conclusions are consistent with the data from alveolar bone defect animal models, and although the EDA exon was excluded in only part of fibroblasts of Cluster 2, the injection of these partly modified fibroblasts still decreased the osteoclasts formation in the location of bone defects, in contrast with the injection of untreated fibroblasts, as well as untreated bone defects. These results further demonstrated that the cells of Cluster 2 are important to various bone destruction. The gene-modified cells have been used to treat lung cancer and β-hemoglobinopathies (Cyranoski, 2016; Traxler et al., 2016); in this study, specific fibroblast subsets may be a new target for artificial modification, by which the cell therapy could also be applied to treat diseases of bone destruction.

In this study, the heterogeneity of fibroblasts was investigated in colonies isolated from the fibrous capsules of radicular cysts, and 2 subsets of cells with distinct osteoclastogenic induction abilities, osteoclastogenesis-related genes expression, and underlying mechanisms were identified. On this basis, the fibroblast colonies of Cluster 2 were found to induce osteoclastogenesis via EDA + FN and VEGF-A, which may be the principal subset of cells that lead to active bone resorption and perhaps have therapeutic applications for treating lesions with bone destruction.

CONFLICT OF INTERESTS

None declared.

AUTHOR CONTRIBUTIONS

Hai-Cheng Wang designed the research; Jingwen Yangand ShuyuXu performed the experiments; Jingwen Yangand ShuyuXu contributed new reagents or analytical tools; Hai-Cheng WangandJingwen Yang analyzed the data; and Jingwen Yang wrote the paper.

ORCID

Hai-Cheng Wang 🆔 https://orcid.org/0000-0001-8189-6424

REFERENCES

Bernardi, L., Visioli, F., Nor, C., & Rados, P. V. (2015). Radicular cyst: An update of the biological factors related to lining epithelium. *J Endod*, *41*(12), 1951–1961. https://doi.org/10.1016/j.joen.2015.08.036

Boda, S. K., Almoshari, Y., Wang, H., Wang, X., Reinhardt, R. A., Duan, B., … Xie, J. (2019). Mineralized nanofiber segments coupled with calcium-binding BMP-2 peptides for alveolar bone regeneration. *Acta Biomaterialia*, *85*, 282–293. https://doi.org/10.1016/j.actbio.2018.12.051

Busch, S., Andersson, D., Bom, E., Walsh, C., Stahlberg, A., & Landberg, G. (2017). Cellular organization and molecular differentiation model of breast cancer-associated fibroblasts. *Molecular Cancer*, *16*(1), 73. https://doi.org/10.1186/s12943-017-0642-7

Cyranoski, D. (2016). CRISPR gene-editing tested in a person for the first time. *Nature*, *539*(7630), 479. https://doi.org/10.1038/nature.2016.20988

de Moraes, M., de Lucena, H. F., de Azevedo, P. R., Queiroz, L. M., & Costa Ade, L. (2011). Comparative immunohistochemical expression of RANK, RANKL and OPG in radicular and dentigerous cysts. *Archives of Oral Biology*, *56*(11), 1256–1263. https://doi.org/10.1016/j.archoralbio.2011.05.009

Driskell, R. R., Lichtenberger, B. M., Hoste, E., Kretzschmar, K., Simons, B. D., Charalambous, M., … Watt, F. M. (2013). Distinct fibroblast lineages determine dermal architecture in skin development and repair. *Nature*, *504*(7479), 277–281. https://doi.org/10.1038/nature12783

Du, W. J., Chi, Y., Yang, Z. X., Li, Z. J., Cui, J. J., Song, B. Q., … Han, Z. C. (2016). Heterogeneity of proangiogenic features in mesenchymal stem cells derived from bone marrow, adipose tissue, umbilical cord, and placenta. *Stem Cell Research & Therapy*, *7*(1), 163. https://doi.org/10.1186/s13287-016-0418-9

Garcia, C. C., Sempere, F. V., Diago, M. P., & Bowen, E. M. (2007). The post-endodontic periapical lesion: Histologic and etiopathogenic aspects. *Medicina Oral, Patología Oral y Cirugía Bucal*, *12*(8), E585–590.

Guerrero-Juarez, C. F., Dedhia, P. H., Jin, S., Ruiz-Vega, R., Ma, D., Liu, Y., … Plikus, M. V. (2019). Single-cell analysis reveals fibroblast heterogeneity and myeloid-derived adipocyte progenitors in murine skin wounds. *Nature Communications*, *10*(1), 650. https://doi.org/10.1038/s41467-018-08247-x

Henriques, A., Silva, I., Inês, L., Souto-Carneiro, M. M., Pais, M. L., Trindade, H., … Paiva, A. (2016). CD38, CD81 and BAFFR combined expression by transitional B cells distinguishes active from inactive systemic lupus erythematosus. *Clinical and Experimental Medicine*, *16*(2), 227–232. https://doi.org/10.1007/s10238-015-0348-3

Johnson, N. R., Gannon, O. M., Savage, N. W., & Batstone, M. D. (2014). Frequency of odontogenic cysts and tumors: A systematic review. *Journal of Investigative and Clinical Dentistry*, 5(1), 9–14. https://doi.org/10.1111/jicd.12044

Johnson, N. R., Savage, N. W., Kazoullis, S., & Batstone, M. D. (2013). A prospective epidemiological study for odontogenic and non-odontogenic lesions of the maxilla and mandible in Queensland. *Oral Surgery, Oral Medicine, Oral Pathology and Oral Radiology*, 115(4), 515–522. https://doi.org/10.1016/j.oooo.2013.01.016

Kawagishi-Hotta, M., Hasegawa, S., Igarashi, T., Yamada, T., Takahashi, M., Numata, S., ... Akamatsu, H. (2017). Enhancement of individual differences in proliferation and differentiation potentials of aged human adipose-derived stem cells. *Regenerative Therapy*, 6, 29–40. https://doi.org/10.1016/j.reth.2016.12.004

Kumra, H., & Reinhardt, D. P. (2016). Fibronectin-targeted drug delivery in cancer. *Advanced Drug Delivery Reviews*, 97, 101–110. https://doi.org/10.1016/j.addr.2015.11.014

Lambrechts, D., Wauters, E., Boeckx, B., Aibar, S., Nittner, D., Burton, O., ... Thienpont, B. (2018). Phenotype molding of stromal cells in the lung tumor microenvironment. *Nature Medicine*, 24(8), 1277–1289. https://doi.org/10.1038/s41591-018-0096-5

Liang, Y., Wen, L., Shang, F., Wu, J., Sui, K., & Ding, Y. (2016). Endothelial progenitors enhanced the osteogenic capacities of mesenchymal stem cells in vitro and in a rat alveolar bone defect model. *Archives of Oral Biology*, 68, 123–130. https://doi.org/10.1016/j.archoralbio.2016.04.007

Liu, C. Y., & Wang, H. C. (2019). The fibroblast of radicular cyst facilitate osteoclastogenesis via the autocrine of Fibronectin containing extra domain A. *Oral Diseases*, 25(4), 1136–1146. https://doi.org/10.1111/odi.13064

Lv, W. Q., Wang, H. C., Peng, J., Wang, Y. X., Jiang, J. H., & Li, C. Y. (2017). Gene editing of the extra domain A positive fibronectin in various tumors, amplified the effects of CRISPR/Cas system on the inhibition of tumor progression. *Oncotarget*, 8(62), 105020–105036. https://doi.org/10.18632/oncotarget.21136

Maridas, D. E., Rendina-Ruedy, E., Le, P. T., & Rosen, C. J. (2018). Isolation, culture, and differentiation of bone marrow stromal cells and osteoclast progenitors from mice. *Journal of Visualized Experiments*, (131) https://doi.org/10.3791/56750

Mizoguchi, F., Slowikowski, K., Wei, K., Marshall, J. L., Rao, D. A., Chang, S. K., ... Brenner, M. B. (2018). Functionally distinct disease-associated fibroblast subsets in rheumatoid arthritis. *Nature Communications*, 9(1), 789. https://doi.org/10.1038/s41467-018-02892-y

Morgan, P. R. (2011). Odontogenic tumors: A review. *Periodontol 2000*, 57(1), 160–176. https://doi.org/10.1111/j.1600-0757.2011.00393.x

Ostman, A. (2014). Cancer-associated fibroblasts: Recent developments and emerging challenges. *Seminars in Cancer Biology*, 25, 1–2. https://doi.org/10.1016/j.semcancer.2014.02.004

Philippeos, C., Telerman, S. B., Oulès, B., Pisco, A. O., Shaw, T. J., Elgueta, R., ... Watt, F. M. (2018). Spatial and Single-Cell Transcriptional Profiling Identifies Functionally Distinct Human Dermal Fibroblast Subpopulations. *The Journal of Investigative Dermatology*, 138(4), 811–825. https://doi.org/10.1016/j.jid.2018.01.016

Raz, Y., Cohen, N., Shani, O., Bell, R. E., Novitskiy, S. V., Abramovitz, L., ... Erez, N. (2018). Bone marrow-derived fibroblasts are a functionally distinct stromal cell population in breast cancer. *Journal of Experimental Medicine*, 215(12), 3075–3093. https://doi.org/10.1084/jem.20180818

Shinde, A. V., Kelsh, R., Peters, J. H., Sekiguchi, K., Van De Water, L., & McKeown-Longo, P. J. (2015). The alpha4beta1 integrin and the EDA domain of fibronectin regulate a profibrotic phenotype in dermal fibroblasts. *Matrix Biology*, 41, 26–35. https://doi.org/10.1016/j.matbio.2014.11.004

Suda, Y., Neri, S., Hashimoto, H., Higuchi, Y., Ishibashi, M., Sugano, M., ... Ishii, G. (2016). Clonal heterogeneity in osteogenic potential of lung cancer-associated fibroblasts: Promotional effect of osteogenic progenitor cells on cancer cell migration. *Journal of Cancer Research and Clinical Oncology*, 142(7), 1487–1498. https://doi.org/10.1007/s00432-016-2171-y

Sukegawa, S., Matsuzaki, H., Katase, N., Kawai, H., Kanno, T., Asaumi, J. I., & Furuki, Y. (2019). Morphological characteristics of radicular cysts using computed tomography. *Odontology*, https://doi.org/10.1007/s10266-019-00443-5

Traxler, E. A., Yao, Y., Wang, Y. D., Woodard, K. J., Kurita, R., Nakamura, Y., ... Weiss, M. J. (2016). A genome-editing strategy to treat beta-hemoglobinopathies that recapitulates a mutation associated with a benign genetic condition. *Nature Medicine*, 22(9), 987–990. https://doi.org/10.1038/nm.4170

Wang, H. C., Jiang, W. P., Sima, Z. H., & Li, T. J. (2015). Fibroblasts isolated from a keratocystic odontogenic tumor promote osteoclastogenesis in vitro via interaction with epithelial cells. *Oral Diseases*, 21(2), 170–177. https://doi.org/10.1111/odi.12231

Wang, H. C., & Li, T. J. (2013). The growth and osteoclastogenic effects of fibroblasts isolated from keratocystic odontogenic tumor. *Oral Diseases*, 19(2), 162–168. https://doi.org/10.1111/j.1601-0825.2012.01966.x

Wang, H. C., Wang, P., Chen, Y. W., & Zhang, Y. (2019). Bevacizumab or fibronectin gene editing inhibits the osteoclastogenic effects of fibroblasts derived from human radicular cysts. *Acta Pharmacologica Sinica*, 40(7), 949–956. https://doi.org/10.1038/s41401-018-0172-x

Wang, H. C., Yang, Y., Xu, S. Y., Peng, J., Jiang, J. H., & Li, C. Y. (2015). The CRISPR/Cas system inhibited the pro-oncogenic effects of alternatively spliced fibronectin extra domain A via editing the genome in salivary adenoid cystic carcinoma cells. *Oral Diseases*, 21(5), 608–618. https://doi.org/10.1111/odi.12323

Xie, T., Wang, Y., Deng, N., Huang, G., Taghavifar, F., Geng, Y., ... Jiang, D. (2018). Single-cell deconvolution of fibroblast heterogeneity in mouse pulmonary fibrosis. *Cell Reports*, 22(13), 3625–3640. https://doi.org/10.1016/j.celrep.2018.03.010

Xu, S. Y., & Wang, Z. L. (2017). Bone marrow mesenchymal stem cell-derived exosomes enhance osteoclastogenesis during alveolar bone deterioration in rats. *RSC Advances*, 7(34), 21153–21163. https://doi.org/10.1039/c6ra27931g

Yang, J. W., Jiang, J. H., Wang, H. C., & Li, C. Y. (2019). The Extra Domain A of fibronectin facilitates osteoclastogenesis in radicular cysts through vascular endothelial growth factor. *International Endodontic Journal*, https://doi.org/10.1111/iej.13241

Zhang, L., & Chan, C. (2010). Isolation and enrichment of rat mesenchymal stem cells (MSCs) and separation of single-colony derived MSCs. *Journal of Visualized Experiments*,(37) https://doi.org/10.3791/1852

Zhao, J. H., Tsai, C. H., & Chang, Y. C. (2014). Management of radicular cysts using platelet-rich fibrin and bioactive glass: A report of two cases. *Journal of the Formosan Medical Association*, 113(7), 470–476. https://doi.org/10.1016/j.jfma.2011.09.027

Zizzi, A., Aspriello, S. D., Ferrante, L., Stramazzotti, D., Colella, G., Balercia, P., ... Rubini, C. (2013). Immunohistochemical correlation between microvessel density and lymphoid infiltrate in radicular cysts. *Oral Diseases*, 19(1), 92–99. https://doi.org/10.1111/j.1601-0825.2012.01961.x